Journal of Power Sources 183 (2008) 49–54

Contents lists available at ScienceDirect

Journal of Power Sources

journal homepage: www.elsevier.com/locate/jpowsour

Polarization measurements of anode-supported solid oxide fuel cells studied by incorporation of a reference electrode

Haiming Xiao[a,*], Thomas L. Reitz[b], Michael A. Rottmayer[b]

[a] Aerospace Power and Propulsion, UES Corporation, 4401 Dayton-Xenia Road, Dayton, OH 45432, USA
[b] Air Force Research Laboratory, Wright Patterson Air Force Base, OH 45433, USA

ARTICLE INFO

Article history:
Received 28 March 2008
Received in revised form 25 April 2008
Accepted 28 April 2008
Available online 13 May 2008

Keywords:
Fuel cell
SOFC
Reference electrode
Polarization
Electrochemical impedance spectroscopy

ABSTRACT

A three-electrode system configuration was applied to an anode-supported solid oxide fuel cell where the anode to cathode surface area ratio was ~7.9, and Ni/YSZ was used as the anode, LSM as the cathode, Pt as the reference electrode, and thin YSZ film as the electrolyte. The cell was polarized potentiostatically at −0.2, −0.4, −0.6 and −0.8 V versus open circuit voltage (OCV) and the potential change versus a reference electrode were recorded to ascertain the relative electrode polarization contributions. The results of these studies suggested that, while the anode contributions to cell polarization were less significant than that observed for the cathode, they were not negligible. Furthermore, the disparity in the relative electrode polarization contribution was observed to decrease with increasing temperature and polarization. Electrode polarization studies suggested that cathodic overvoltage decreased remarkably with increasing temperature whereas anodic overvoltage increased slightly with increasing temperature. Electrode kinetic parameters were extracted from these polarization experiments and the implications of these parameters to cell performance were discussed. Lastly, electrochemical impedance spectroscopy (EIS) data was presented to further elucidate the relative contributions of the anode and cathode impedances on button cell performance.

1. Introduction

Solid oxide fuel cells (SOFC) appear to be a promising candidate for stand-alone power sources since operating efficiencies can approach 70% under certain conditions while emitting relatively benign byproducts. Recently, interest in SOFCs has increased significantly due to studies which suggest potential operation on hydrocarbon fuels including propane and butane [1,2]. Among the SOFCs, anode-supported cells have received much attention because they employ thin electrolyte films thus providing higher power densities due to lower ohmic resistances than comparable electrolyte-supported configurations. These thin electrolyte film cells also allow for reduced SOFC stack working temperatures thus decreasing some of the material challenges associated with high temperature sealing and current collection [3].

In SOFC research, button cells are normally used to study the fundamental electrochemical processes and the results of these studies are taken as the basis for improving full or intermediate scale cells. Therefore, any improvement to the methodology of the button cell study can have far-reaching consequences in development of full-scale cell-stacks. In the electrochemical study of aqueous solutions or molten salts, a three-electrode system including working electrode, auxiliary electrode and reference electrode is commonly used [4]. The advantage of using a three-electrode system is that each electrode (i.e. cathode or anode) can be examined separately with little interference from its counter electrode and with minimal ohmic (IR) contributions. However, in the examination of SOFCs, a three-electrode system has not been widely adopted due to the intractability of reference electrode placement within the solid-state electrolyte. While several studies have been published regarding the inclusion of reference electrodes into solid-state systems, there remains considerable controversy regarding proper placement in order to ensure that the reference observes a uniform current distribution [5–10]. In one particular example it is demonstrated through calculation that a three-electrode arrangement for electrolyte-supported SOFCs can be achieved by placing the reference around the periphery of the solid electrolyte support. In this approach it is argued that the reference electrode observes completely uniform current distribution when placed between two symmetric electrodes [9]. Other authors have suggested or tested alternative configurations, however most, if not all, of these approaches are impractical for anode-supported cells with thin electrolyte (~10 μm) layers. For anode-supported cells, the vast majority of studies are conducted without refer-

* Corresponding author. Tel.: +1 937 255 5462.
E-mail address: Haiming.Xiao@wpafb.af.mil (H. Xiao).

0378-7753/$ – see front matter © 2008 Elsevier B.V. All rights reserved.
doi:10.1016/j.jpowsour.2008.04.088

ence electrodes, making determination of the relative electrode performances difficult [11,12]. In many of these studies, EIS is used to provide insight into each of the electrode processes. However, EIS data is notoriously difficult to interpret because many of the electrochemical processes (redox reactions, diffusion, conductivity, etc.) cannot be completely separated in the time domain and result in distributed impedances in the spectra. As such, reference electrodes can be utilized to compliment EIS data as a means to separate individual electrode performance. In this way, the polarization contributions from the bulk anode, cathode and electrolyte can be distinguished from each other during cell operation.

In the present work, a three-electrode configuration was applied to an anode-supported solid oxide fuel cell to elucidate the contributions to the cell impedances associated with the anode and cathode electrodes. Polarization experiments were used to extract relevant electrochemical kinetic parameters at different cell operating temperatures.

2. Experimental

Fabrication of the five-layer, anode-supported button cells was described previously [13]. To summarize briefly, the samples were prepared by lamination of multiple layers of tape-cast green films to produce an anode-supported substrate (~600 μm) with an anode functional layer (~15 μm) and thin film YSZ electrolyte (~10 μm). A green sample 3.20 cm in diameter was cut from the laminated tape with a laser cutter (Universal Laser Systems) and co-sintered at 1400 °C for 2 h. A LSM and YSZ paste was then applied to the YSZ electrolyte, followed by a layer of a pure LSM paste. The cell was then fired at 1200 °C for 1 h. After processing, the area of the cathode was ~0.62 cm^2 with a nominal thickness of ~30 μm. A platinum reference electrode was then pasted on the YSZ surface at the cathode side as the reference electrode. In order to minimize IR drop between the cathode and the reference electrode, the distance between the two electrodes was minimized. Platinum was chosen as the reference electrode because it exhibits good stability, reproducibility, and reversibility and has been used in related applications such as zirconia-based high temperature oxygen sensors [14]. A profile of a typical three-electrode cell configuration and a picture displaying the frontal view of an actual cell (pre-test) is shown as Fig. 1.

Four Platinum leads were attached to the cell (2-anode, 1-cathode, and 1-reference) and sealed onto an alumina tube (Vesuvius) using high temperature cement (Cerambond 516, Aremco Products Inc.) with the anode side facing the tube. The inside diameter of the alumina tube, which determines the effective anode surface area facing hydrogen fuel, was ~1.9 cm. A specially designed quartz test fixture for feeding fuel gas and releasing exhaust gas was connected to the alumina tube through a compression fitting (Swagelok). Sealing around the anode leads was accomplished through two threaded bushings with silicon rubber septa (ACE Glass) which were attached to the quartz fixture via a graded seal. The complete cell was then placed into the isothermal zone of a clam-shell furnace. Reduction of the NiO to Ni was achieved through a controlled temperature ramp in an anode flow stream of 5% H_2, balance N_2. After the anode reduction was complete, the cell was brought to the desired temperature for testing and the reactant gas was switched to pure hydrogen gas. The cathode chamber is not sealed so a purified air stream was blown over the electrode surface to ensure ample oxygen availability. Electrochemical polarization and characterization was conducted using a Solartron 1260 impedance gain/phase analyzer coupled to a Solartron 1287 electrochemical interface. Two Keithley multimeters (model 175) were used to measure the potentials of the anode and the cathode versus the reference electrode independently. The ratio of the anode to cathode surface area ratio was ~7.9.

3. Results and discussion

The cell used as the basis for the majority of this manuscript produced an OCV of 1.098 V at 750 °C and the potentials of the anode and the cathode versus the reference electrode were −1.064 V and +0.034 V, respectively. It should be noted that the difference of the cathode potential and the anode potential is equal to the observed OCV. Cell polarization experiments were conducted potentiostatically wherein the potential was adjusted in 200 mV intervals relative to the OCV for a maximum polarization of 800 mV. During these tests, the polarization of the anode and cathode were measured independently with respect to the reference electrode. The results of these measurements at different temperature regions are presented in Table 1. It should be noted that, according to the cell configuration shown in Fig. 1, the measured anode potentials versus the reference electrode (listed in the fourth column of Table 1) includes the ohmic voltage drop across the electrolyte, which must be accounted for through the subtraction of IR, where I is the cell current at a given polarization and R is the resistance of the electrolyte. R can be calculated from the following equation:

$$R = \frac{1}{\sigma}\frac{l}{(1/4)\pi d^2} \quad (1)$$

where σ is the conductivity of YSZ electrolyte at a given temperature (e.g., 0.013 Ω^{-1} cm^{-1} at 750 °C and 0.030 Ω^{-1} cm^{-1} at 800 °C), l is the thickness of the electrolyte film (~10 μm), and d is the diameter of the electrolyte (2.50 cm). The calculated values for the ohmic voltage drop across the electrolyte for each case of the polarization experiments are also presented in Table 1. It must be further noted that IR contributions from the anode and cathode electrodes as well as the cathode lead (1-wire used for cathode V and I) were not specifically segregated in these experiments.

From Table 1, it is apparent that the cathodic polarizations are far greater than that observed for the anode. As temperature increases, cathode polarization relative to the anode contribution decreases which can be attributed to both increased kinetics of the oxygen reduction reaction and increased conductivity of the LSM cathode current collector. Conversely, the overpotential of the anode is observed to increase with increasing temperature suggesting that increases in hydrogen oxidation rates or reactant diffusion are offset by the conductivity decrease of the nickel current collector. Contributions from the electrolyte are relatively minor, typical of anode-supported cell configurations.

One obvious reason for the disparity between the anode and cathode overpotentials discussed previously is associated with the large difference in electrode surface area. For anode-supported configurations, it is experimentally challenging to construct electrodes which are equivalent in surface area or are symmetric such that uniform current distributions are achieved. In this study, the significance of the large difference between the anode and the cathode surface area on the observed polarization results must not be overlooked. In order to provide some insight into the disparity in electrode surface area, the data contained in Table 1 were normalized by the electrode surface area ratio of 7.9 for the experiment conducted at 750 °C. These normalized results are presented in Table 2. After normalization it is apparent that some of the difference between the electrode overpotentials has been reduced with anode overpotential steadily increasing in its relative contribution. In general, while observed cathode overpotential increases as a function of cell polarization, the relative contribution of the cathode compared to the anode decreases. This is presumably due

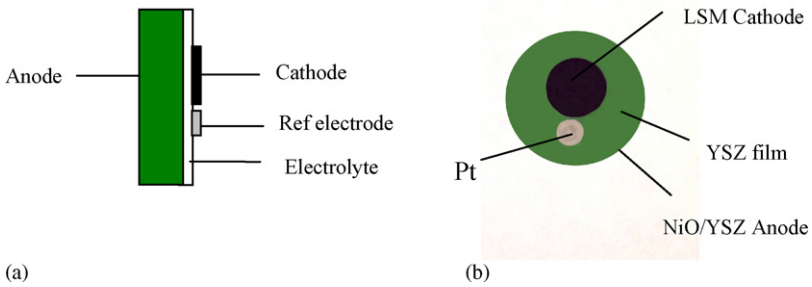

Fig. 1. Diagram (a) and picture (b) of a typical anode-supported button cell with Pt reference electrode.

Table 1
SOFC cathode and anode polarizations (with the surface area ratio of anode to cathode = 7.90) determined via reference electrode for varying controlled cell polarizations at different temperatures

	Cell polarization vs. OCV	Cathode Polarization vs. Ref.		Anode Polarization vs. Ref.		Electrolyte IR Contribution
	Potential (V)	Potential (V)	% Total	Potential (V)	% Total	Potential (mV)
750 °C	0 (1.098 V)	0	–	0	–	0
	−0.200	0.182	91.0	0.014	7.0	1.0
	−0.400	0.369	92.3	0.030	7.5	2.4
	−0.600	0.547	91.2	0.051	8.5	3.9
	−0.800	0.727	90.9	0.072	9.0	6.0
800 °C	0 (1.080 V)	0	–	0	–	0
	−0.200	0.168	84.4	0.021	10.5	0.9
	−0.400	0.347	86.7	0.038	9.5	2.0
	−0.600	0.530	88.4	0.066	11.0	3.1
	−0.800	0.707	88.0	0.096	12.0	4.1
850 °C	0 (1.067 V)	0	–	0	–	0
	−0.200	0.169	79.9	0.049	24.5	0.7
	−0.400	0.319	79.7	0.093	23.3	1.6
	−0.600	0.478	79.6	0.133	22.2	2.5
	−0.800	0.612	76.5	0.203	25.4	3.2

to the relative difficulty of the desorption and transport of steam from the anode active layer, especially at higher current densities. It must be noted that this normalization treatment through sole consideration of electrode geometry is not adequate to understand the relative contributions of the individual electrodes. To fully understand these contributions, a more careful normalization procedure must be used which attempts to incorporate features of the microscopic active region as well as the electrode dynamics during polarization. Lastly, it must be understood that the asymmetry in this study, both in electrode placement and in relative electrode size, likely contributes to a degree of uncertainty. Studies are underway to clarify this uncertainty through alternative reference electrode placement and will be the subjects of future manuscripts. Regardless, it is clear that the relative contributions of the electrodes to button cell performance change as a function of cell polarization.

Steady-state polarization experiments were conducted to independently evaluate the cathode and the anode as the working electrode with respect to the reference electrode. Anodic and cathodic polarization curves were obtained where IR drop between the electrode of interest and the reference electrode was compensated or eliminated using the current interrupt method. Therefore, the influence of a non-uniform current distribution on the measured IR polarization results was minimized. Literature has stressed the importance of proper reference electrode placement in ensuring that uniform current distribution is sampled [5,6]. However, IR compensation techniques can be used to mitigate much of the error associated with utilizing asymmetric electrode configurations The implication is that the benefits of reference electrodes in clarifying electrode performance outweighs the potential errors associated with improper placement; the uncertainties of which can be offset through common experimental techniques.

Polarization experiments were performed to evaluate the relative contributions of the anode and cathode at constant temperature and the data is shown as Fig. 2. For this cell geometry it can be observed that the cathode has a far larger polarization than the anodic process for any cell current, which is in good agreement with the results from the polarized cell voltage distribution measurements, presented earlier (Table 1).

Table 2
Normalized data from Table 1 compensating for dissimilar anode and cathode active areas measured at 750 °C

	Cell polarization vs. OCV	Cathode polarization vs. ref. (cathode surface area normalized)		Anode polarization vs. ref. (anode surface area normalized)	
	Potential (V)	Potential (V)	% Total	Potential (V)	% Total
750 °C	0 (1.098 V)	0	–	0	–
	−0.200	0.124	62.2	0.076	37.8
	−0.400	0.244	60.9	0.156	39.1
	−0.600	0.346	57.6	0.254	42.4
	−0.800	0.449	56.1	0.351	43.9

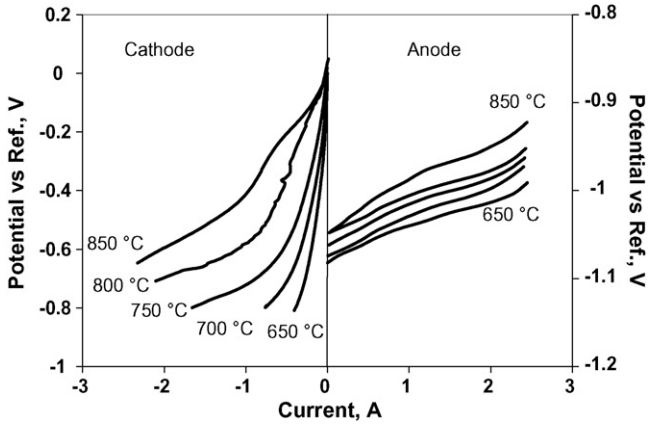

Fig. 2. Cathodic and anodic polarization vs. platinum reference electrode at different temperatures for an anode-supported button cell with anode to cathode surface area ratio of 7.9.

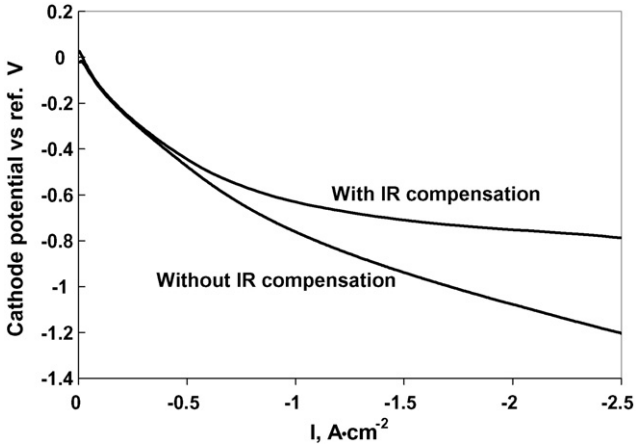

Fig. 4. Cathodic polarization curves vs. platinum reference electrode at 750 °C.

Further clarification of the cell performance can be obtained when the data from Fig. 2 is replotted as cell overpotential as a function of electrode current density (Fig. 3). From this figure it is apparent that the overvoltage of the cathode overwhelms that of the anode at lower temperatures (650–750 °C). However, the difference between the cathode overvoltage and the anode overvoltage at equivalent current density decreases dramatically with increasing temperature. Furthermore, Fig. 3 clearly displays the striking dissimilarity between anode and cathode behavior. While the Ni–YSZ anode shows a nearly linear polarization with electrode current density, the LSM cathode exhibits two distinct regions. At lower overpotentials, it is evident that the LSM cathode presents higher activation resistance which is observed to decrease as the overpotential increases. This behavior was most apparent at higher operating temperature (750–850 °C). In literature, this phenomenon has been thoroughly discussed and has been associated with the reduction of the LSM perovskite especially at higher operating temperature. This reduction is thought to increase the number of oxygen vacancies thus increasing the mixed-conducting properties of the LSM electrode under polarization and is observed predominately at temperatures over 700 °C [15–17]. It is also apparent from Fig. 3 that while the cathodic overvoltage decreased remarkably with increasing temperature, the anodic overvoltage increased noticeably with temperature. This behavior could be attributed in part to an increase in the resistivity of the Ni–YSZ cermet associated with the drop in metallic conductivity with increasing temperature. However, calculation of the electrode ohmic drop associated with the resistivity of the nickel does not provide for a reduction of this magnitude ($R_{\text{nickel, 650°C}} \sim 4\,\mu\Omega$). It is possible that additional factors must be contributing to the increase in anode overpotential with temperature. As such, from the point of view of the Ni/YSZ anode, lower working temperatures are favored providing yet another motivation for lower cell operating temperatures in SOFC design.

Experiments were conducted wherein the cathode was polarized relative to the reference electrode to explore the magnitude of the cell ohmic contribution and the data is presented as Fig. 4. It can be observed that at lower current densities the two curves are overlapping, suggesting that a negligible IR drop occurs between the cathode and reference electrodes. At high current densities, however, the difference between the two curves becomes more significant indicating that the ohmic contribution is substantial under these conditions. Data for the LSM cathode operating at 750 °C relative to the platinum reference is expressed in terms of overvoltage versus logarithm of current density and is presented in Fig. 5. It can be observed that this data does not yield a linear region typical of Tafel kinetics. This observation is consistent with a multi-step or mechanism change and can be attributed to the reduction of the cathode at elevated temperatures and with the complexity of the oxygen reduction reaction.

To assess the nature of the anode kinetics, the anode polarization data is plotted in terms of overvoltage versus logarithm of current density and the results presented as Fig. 6. Unlike that which was

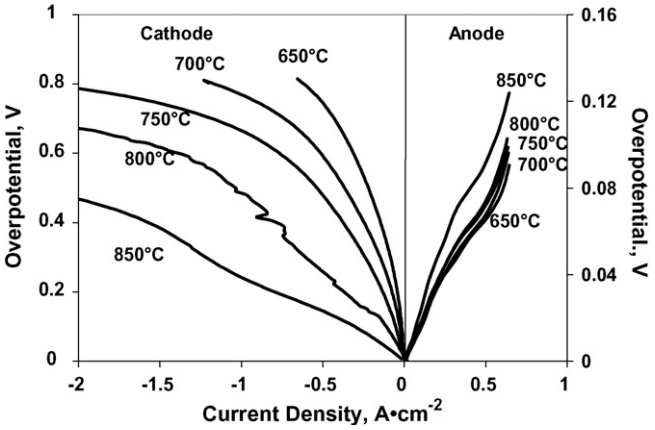

Fig. 3. Cathodic and anodic overvoltages as a function of current density at different temperatures.

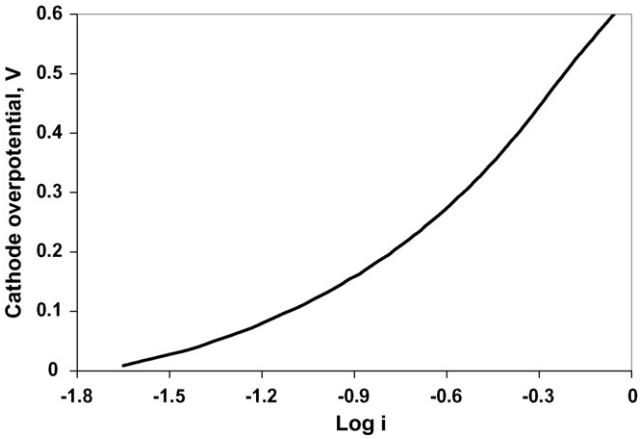

Fig. 5. Plot of cathodic overvoltage vs. the logarithm of current density at 750 °C.

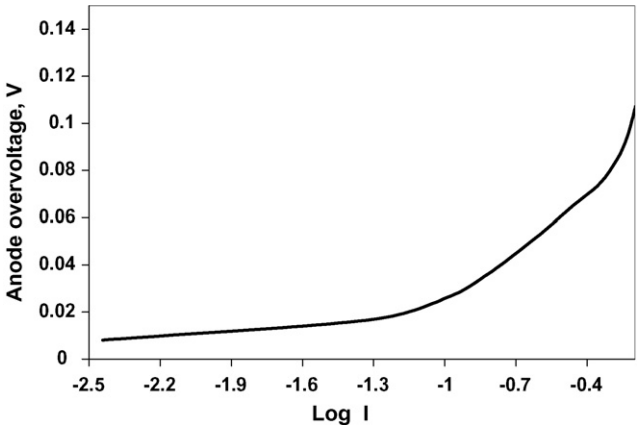

Fig. 6. Plot of anodic overvoltage vs. logarithm of current density at 750 °C.

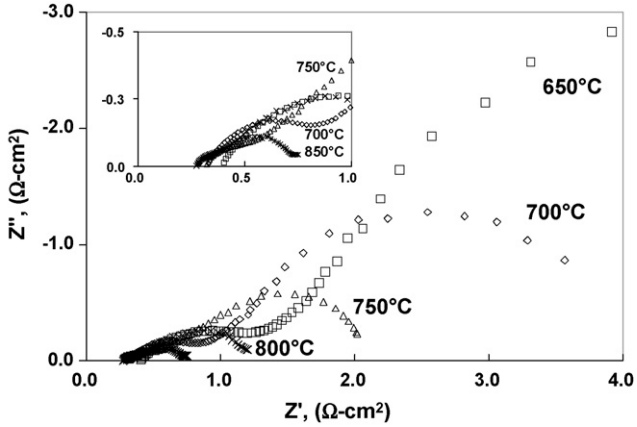

Fig. 7. Cell impedance spectra obtained at open circuit voltage for different temperatures (□) 650 °C, (◊) 700 °C, (△) 750 °C, (×) 800 °C and (✱) 850 °C.

observed for the cathode (Fig. 5), the Tafel plot for the anode yields a straight line in the current density range of 0.1–0.3 A cm^{-2} with slope of 0.0813 and intercept of 0.1035. This is characteristic of charge-transfer kinetics according to the Tafel equation (Eq. (2)):

$$\eta = -\frac{RT}{\alpha nF}\ln i^0 + \frac{RT}{\alpha nF}\ln i = -b\log i^0 + b\log i \quad (2)$$

After fitting the data from each of the anode polarization experiments to (2), the exchange current density (i^0), the charge-transfer coefficient (α), and the Tafel slope (b) were obtained. Tafel parameters for the Ni–YSZ electrode as a function of temperature are presented in Table 3.

The kinetic data obtained clearly shows a decrease in the observed anode oxidation kinetics as a function of temperature with the exchange current density decreasing from 59.9 mA cm^{-2} at 650 °C to 53.7 mA cm^{-2} at 850 °C. Concurrently, an increase in the Tafel slope is observed from 68.7 mV dec^{-1} measured at 650 °C to 100.1 mV dec^{-1} at 850 °C. These data clearly indicate a strong dependence of the anode oxidation kinetics with temperature. As such, it is a combination of both kinetic factors and anode conductivity contributions that account for the decrease in activity as a function of temperature.

EIS experiments were conducted to further clarify the relative contributions of the electrodes. It has been shown that, through careful experimentation, EIS spectra can be deconvoluted to provide insight into the electrode processes occurring in anode-supported button cells [12]. EIS spectra as a function of cell temperature are presented as Fig. 7. From these plots it can be seen that the cell area specific ohmic resistance (ASOR) reduces noticeably with temperature corresponding to an increase in the ionic conductivity of the YSZ electrolyte and electrode functional layers. The ASOR values are extracted from the first real intercept of the EIS spectrum and are indicative of the total ohmic cell resistance including electrodes, electrolyte, electrode contacts and current collectors. Because of the limited area of the cathode in these experiments, only 1 lead was attached to the cathode so all EIS experiments were conducted in 3-probe mode (2-anode, 1-cathode). As such, a portion of the ASOR is associated with the cathode current collector and lead. ASOR values for the cell decrease from 0.40 Ω cm^2 measured at 650 °C to 0.27 Ω cm^2 at 800 °C or 33%. No further decrease in the ASOR was observed when the cell temperature was raised to 850 °C suggesting that the increased resistivity of the metallic components are offsetting the increase in ionic conductivity of the ceramic conductors. In previous papers, it has been demonstrated that cathode and anode-specific impedances can be attributed to the individual semi-circular features in the EIS spectra of anode-supported button cells [12,11]. Based on these references, it is assumed that the first and last semi-circular arcs contained in Fig. 7 are associated with anode-specific and cathode-specific electrode processes, respectively. As such, it can be seen that the relative contributions of the cell impedance from the cathode-specific processes decrease compared to anode specific impedances as a function of cell temperature.

Table 3
Electrode kinetic parameters for Ni–YSZ anode

Temperature (°C)	Tafel slope (mV dec^{-1})	Electron transfer coefficient	Exchange current (mA cm^{-2})
650	68.7	0.67	59.9
700	84.1	0.54	67.7
750	87.3	0.52	58.1
800	91.2	0.50	57.5
850	100.1	0.46	53.7

EIS experiments as a function of cell polarization at constant temperature (750 °C) were also performed and the data is presented in Fig. 8. Again it is apparent that the later semi-circular arc is far greater initially, but then decreases with increasing polarization until the relative impedances are nearly equivalent. These data suggest that the cathodic-specific impedances decrease disproportionately with polarization compared to the anode (first semicircle). The findings from the EIS spectra, both as a function of temperature and polarization, clearly compliment the previously discussed

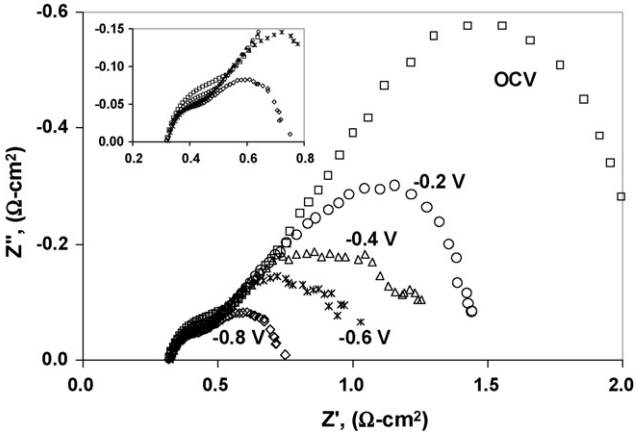

Fig. 8. Cell impedance spectra obtained as a function of polarization measured at 750 °C: (□) OCV, (✱) −0.2 V, (△) −0.4 V, (✱) −0.6 V and (◊) −0.8 V.

reference electrode experiments which showed a relative reduction in the cathodic overpotential compared to the anode (Tables 1 and 2).

4. Conclusions

Polarization experiments of an anode-supported SOFC incorporating a platinum reference electrode in an asymmetric arrangement were performed to clarify the relative contributions of the electrode impedances on cell performance. These experiments revealed that the relative polarization of the cathode was significantly higher than that of the anode for low cell overpotentials and temperatures. However, the relative overpotential of the cathode decreased relative to the anode as cell polarization and temperature were increased. This observation is associated with an increase in the mixed conducting properties of the composite cathode due to an increase in the number of oxygen vacancies in the LSM lattice. The polarization data suggests that the overpotentials for the anode are not insignificant and become an increasing portion of the total cell impedance as both polarization and temperature increase. As was discussed, these increases are not sufficiently explained by thermally induced decreases in electronic conductivity of the nickel component but are due to some larger decrease in electrocatalytic behavior.

Cell EIS spectra provide additional clarity to the nature of the electrode impedances. The trends observed in these data were in good agreement with the polarization experiments with reductions in the cathode impedances outweighing the anode. However, again it is observed that the relative magnitude of the anode contributions to the cell impedance become quite significant especially at higher temperatures and polarization.

Future study to understand the relative error introduced as a result of the asymmetric electrode configuration and the dissimilarity in electrode active area is planned.

References

[1] C. Lu, W.L. Worrell, C. Wang, S. Park, H. Kim, J.M. Vohs, R.J. Gorte, Solid State Ionics 152/153 (2002) 393–397.
[2] Z. Zhan, J. Liu, S. Barnett, Appl. Catal. A: Gen. 262 (2004) 255–259.
[3] F. Zhao, A. Virkar, J. Power Sources 141 (2005) 79–95.
[4] A.J. Bard, L.R. Faulkner, Electrochemical Methods: Fundamentals and Applications, Wiley, New York, 1980.
[5] J. Winkler, P.V. Hendriken, N. Bonanoos, M. Taylor, M.A. Mogensen, J. Electrochem. Soc. 145 (1998) 1184–1192.
[6] S.B. Adler, J. Electrochem. Soc. 149 (2002) E166–E172.
[7] A. Hashibon, S. Raz, I. Riess, Solid State Ionics 149 (2002) 167–176.
[8] V.V. Krishnan, S. McIntosh, R.J. Gorte, J.M. Vohs, Solid State Ionics 166 (2004) 191–197.
[9] J. Rutman, I. Riess, Electrochim. Acta 52 (2007) 6073–6083.
[10] S.P. Jiang, W. Wang, Electrochem. Solid-State Lett. 8 (2) (2005) A115–A118.
[11] N. Wagner, W. Schnurnberger, B. Muller, M. Lang, Electrochim. Acta 43 (1998) 3785–3793.
[12] T. Reitz, H. Xiao, J. Power Sources 161 (2006) 437–443.
[13] T.L. Reitz, H. Xiao, M. Rottmayer, T. Seibert, ECS Trans. 7 (1) (2007) 687–696.
[14] C. Mallika, O.M. Sreedharan, R. Subasri, J. Eur. Ceram. Soc. 20 (2000) 2297–2313.
[15] J.V. Herle, A.J. McEnvoy, K.R. Thampi, Electrochem. Acta 41 (9) (1996) 1447–1454.
[16] A. Hammouche, E. Siebert, A. Hammou, Mater. Res. Bull. 24 (1989) 367–380.
[17] J.Y. Yi, G.M. Choi, J. Eur. Ceram. Soc. 24 (2004) 1359–1363.